NASA CONTRACTOR REPORT

NASA CR-495

A SUBMILLIMETER INTERFERENCE SPECTROMETER: CHARACTERISTICS, PERFORMANCE AND MEASUREMENTS

by K. H. Breeden, W. K. Rivers, and A. P. Sheppard

Prepared by
GEORGIA INSTITUTE OF TECHNOLOGY
Atlanta, Ga.
for

NATIONAL AERONAUTICS AND SPACE ADMINISTRATION • WASHINGTON, D. C. • MAY 1966

A SUBMILLIMETER INTERFERENCE SPECTROMETER: CHARACTERISTICS, PERFORMANCE AND MEASUREMENTS

By K. H. Breeden, W. K. Rivers, and A. P. Sheppard

Prepared under Grant No. NsG-258 by
GEORGIA INSTITUTE OF TECHNOLOGY
Atlanta, Ga.

for

NATIONAL AERONAUTICS AND SPACE ADMINISTRATION

For sale by the Clearinghouse for Federal Scientific and Technical Information
Springfield, Virginia 22151 – Price $2.00

A SUBMILLIMETER INTERFERENCE SPECTROMETER: CHARACTERISTICS, PERFORMANCE AND MEASUREMENTS

K. H. Breeden, W. K. Rivers, and A. P. Sheppard

ABSTRACT

An interference spectrometer facility for use in the frequency region 40 to 3000 GHz (7.5 mm to 100 μ wavelength) is described. The spectrometer resolution is limited to no less than 0.5 GHz over this range. Results are given of measurements on water vapor absorption in the 500 to 1500 GHz frequency band including a high resolution spectrum from 900 to 1000 GHz. The use of the instrument to measure dielectric constant and loss tangent of materials is described. Also included are discussions of sources, filters and detectors used and of procedures for operating this instrument.

TABLE OF CONTENTS

LIST OF FIGURES

LIST OF TABLES

I. INTRODUCTION

An interference spectrometer has been constructed for the frequency region 40 to 3000 GHz (7.5 mm to 100 μ wavelength) which has unusually high resolution for the region. The spectrometer has been used to measure absorption in gases, dielectric constant and loss tangent of solids, and the frequency response of filters. The development of the spectrometer facility has also produced useful contributions to millimeter and submillimeter component technology.

The interference modulation principle of spectroscopy was first proposed by Michelson in 1891 [2].* Technological improvements were necessary, however, before widespread use could be made, and the modern movement was not begun until around 1950 by P. Fellgett [3]. Popular use in this country has resulted largely from the work and lucid papers of John Strong and his associates [4,5,6].

In an interference spectrometer, the radiation is divided into two equal intensity beams, and a variable path delay is introduced into one of the beams. The two parts are then added together and detected. The detector output as a function of the path delay, called the interferogram, is the direct output of the spectrometer. Because this interferogram is the longitudinal correlation function of the electromagnetic radiation, it follows that the power spectrum can be obtained from it by Fourier transformation, which in the present instance is performed on a digital computer.

The principal advantage of the interference spectrometer is that for each spectral element the integration time is the full recording time of the inteferogram so that the signal-to-noise ratios are high. In addition, signal-to-noise ratios are increased because beams of large solid angle, that is beams with many spatial diffraction modes or degrees of freedom, are allowed. This is a strong advantage in the submillimeter region. Other useful features include relative freedom from effects of energy at out-of-band frequencies and the possibility of apodization or control of the spectral window function.

The instrument facility described in this report includes sources and detectors covering the range 40 to 3000 GHz consisting of neon and argon

*Numbers in square brackets refer to the bibliography.

low-pressure positive column discharge tubes, a high-pressure mercury arc tube, a 1350° K furnace, and waveguide mounted barretter and cryogenic germanium bolometers. Interferometer optics are available for a unique wavefront-dividing arrangement as well as the conventional Michelson configuration. Resonant Mylar beamsplitters are available in a wide range of thicknesses. Automatic digital readout and recording equipment are used for efficient handling of the output data for computer processing.

Many of the development problems and design of the instrument and its components were described in a previous technical report [1]. The present report emphasizes the characteristics and capabilities of the facility, which resulted from the development program sponsored by the National Aeronautics and Space Administration under Research Grant NsG-258. Described herein are results obtained on the spectra of water vapor which indicate the magnitude of error in many theoretical calculations performed in recent years and agree with others. The use of the spectrometer to measure dielectric constant and loss tangent of materials is treated briefly. Also included are comments on the relative efficiency of sources and on the cryogenic bolometer used with the spectrometer. An appendix is included which outlines the fundamentals for operating this particular instrument.

II. SOURCE COMPARISON

A primary limitation to extending operation of the spectrometer over the very wide frequency band from 40 to 3000 GHz and to operating with both a wavefront-dividing interferometer and a Michelson arrangement has been that of finding a suitable noise source. A number of experiments have been performed to find the best available source for each frequency band and interferometer arrangement, and the use of black photographic paper as a low-pass filter to eliminate unwanted energy at high frequencies has been explored.

Preliminary experiments performed in the 40 to 80 GHz frequency band utilized a wavefront-dividing interferometer [1] which fully modulated only energy propagating in the lowest order mode plane wave. The detector used at these low frequencies was an evacuated barretter* and the noise source most frequently used was a low-pressure neon positive column noise source with an effective temperature in the RG-98/u waveguide band of 14,700° K, according to the manufacturer.** In an attempt to verify the prediction that only the lowest order plane wave would be fully modulated in the wavefront-dividing interferometer, a positive column neon tube was mounted in a circular horn and used as an extended area multiple mode source. This source configuration was found to give a modulation efficiency less than 10% as compared with 90% modulation efficiency observed with the waveguide mounted noise source. The wavefront-dividing interferometer modulates energy in spacial modes which have even symmetry about a longitudinal-vertical plane out of phase with energy in those modes with odd- or anti-symmetry. There are two possible methods to overcome the reduction in modulation efficiency resulting from having waves with both symmetries propagating in the optical system. One is to selectively reject the modes with odd symmetry. Practically this can only be done by rejecting all modes higher in order than the fundamental lowest order or plane wave mode. Brief experiments with simple mode selecting

* PRD Electronics holder type 634 with PRD type 632 or MSI Electronics type 134 barretters.

**Roger White Electron Devices type GNW-18-V.

filters indicated that such devices would probably have prohibitively high loss at the higher frequencies.

The other approach to improving modulation efficiency in experiments which necessitate the use of extended area sources (such as radiometry) is to replace the wavefront-dividing interferometer with a Michelson beamsplitter. Such a beamsplitter was constructed of Mylar sheet and the interferometer configuration was changed to the classical Michelson arrangement shown in figures 1 and 2. With the Mylar beamsplitter, modulation efficiency in the 40 to 80 GHz region was 97% with the waveguide mounted neon source and about 95% with the extended area source. The 4 db measured transmission loss of the Michelson arrangement was also slightly better than the 5 db loss of the wavefront-dividing arrangement. Other noise sources tested in the 40 to 80 GHz frequency band with the Michelson interferometer arrangement were a 250-watt mercury arc lamp and a positive-column argon tube. The neon sources were found to be superior to other sources tested, and it was found that impedance matching or emissivity was improved by a few percent when the neon tube was mounted in waveguide so that virtually all of the energy was propagated in a single spatial mode.

In extending the operating frequency to submillimeter wavelengths, the evacuated barretter was replaced by a liquid helium cooled germanium bolometer* and again a number of noise sources were tested. Results obtained with the mercury arc lamp and a 1350° K crucible type oven were better than results from the other noise sources tested at frequencies above 300 GHz. Thus far, the mercury arc noise source has been used more frequently than the crucible because of mechanical and heat transfer problems. It has been found, however, that fluctuations in the effective temperature of the mercury arc source limit the output signal-to-noise ratio to a value considerably lower than the inherent detector noise limitation, whereas the thermal drift of the crucible is small and slow. Thus, the crucible type oven should provide a substantially greater S/N than that observed with the mercury arc source.

Spectra taken with these noise sources are shown in figure 3 over a frequency range from 200 to 650 GHz and under normal atmospheric conditions.

*Texas Instruments CLF-1 Cryoflask.

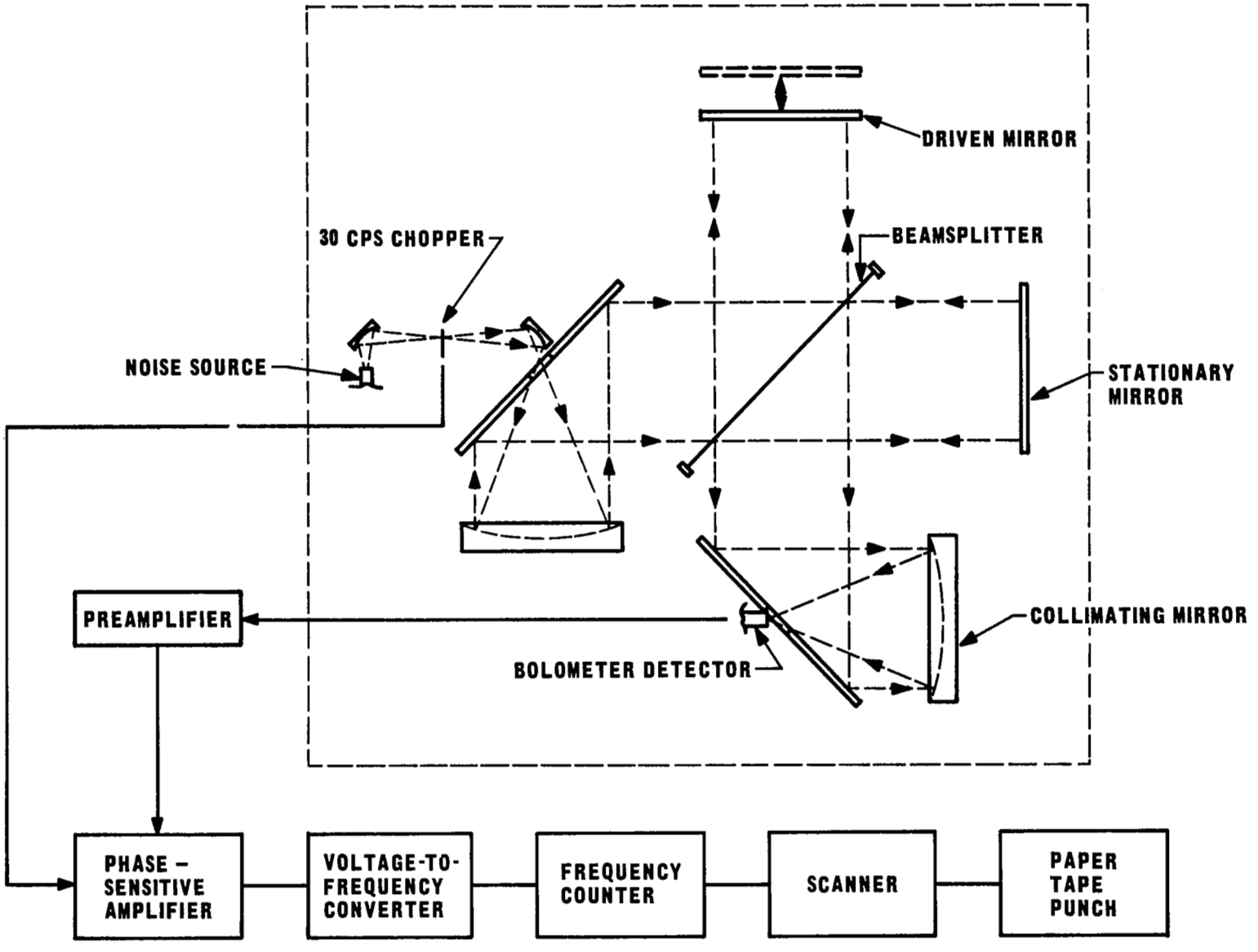

Figure 1. Schematic of Spectrometer and Block Diagram of Output and Data Recording Equipment.

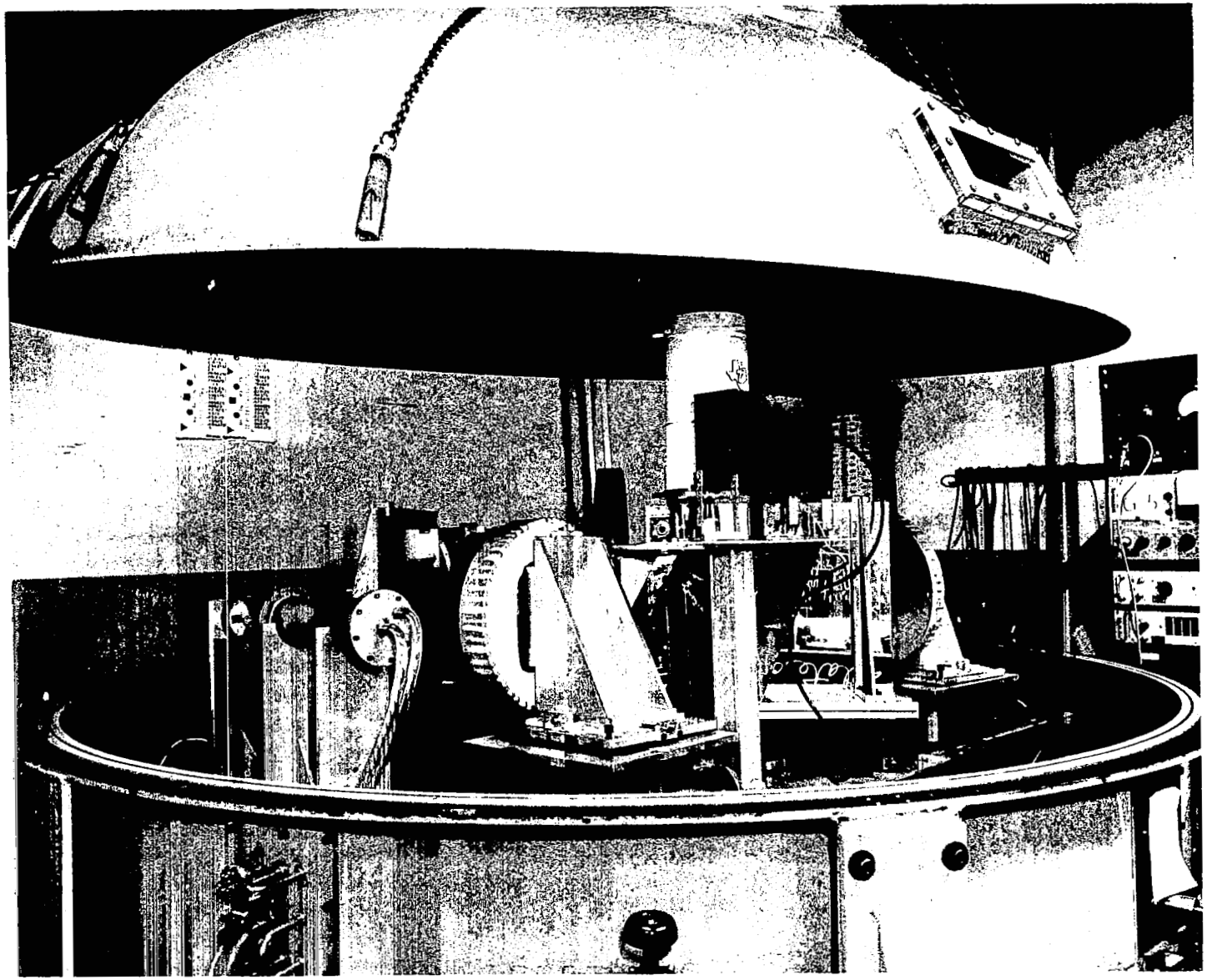

Figure 2. Photograph of the Spectrometer in Vacuum Chamber.

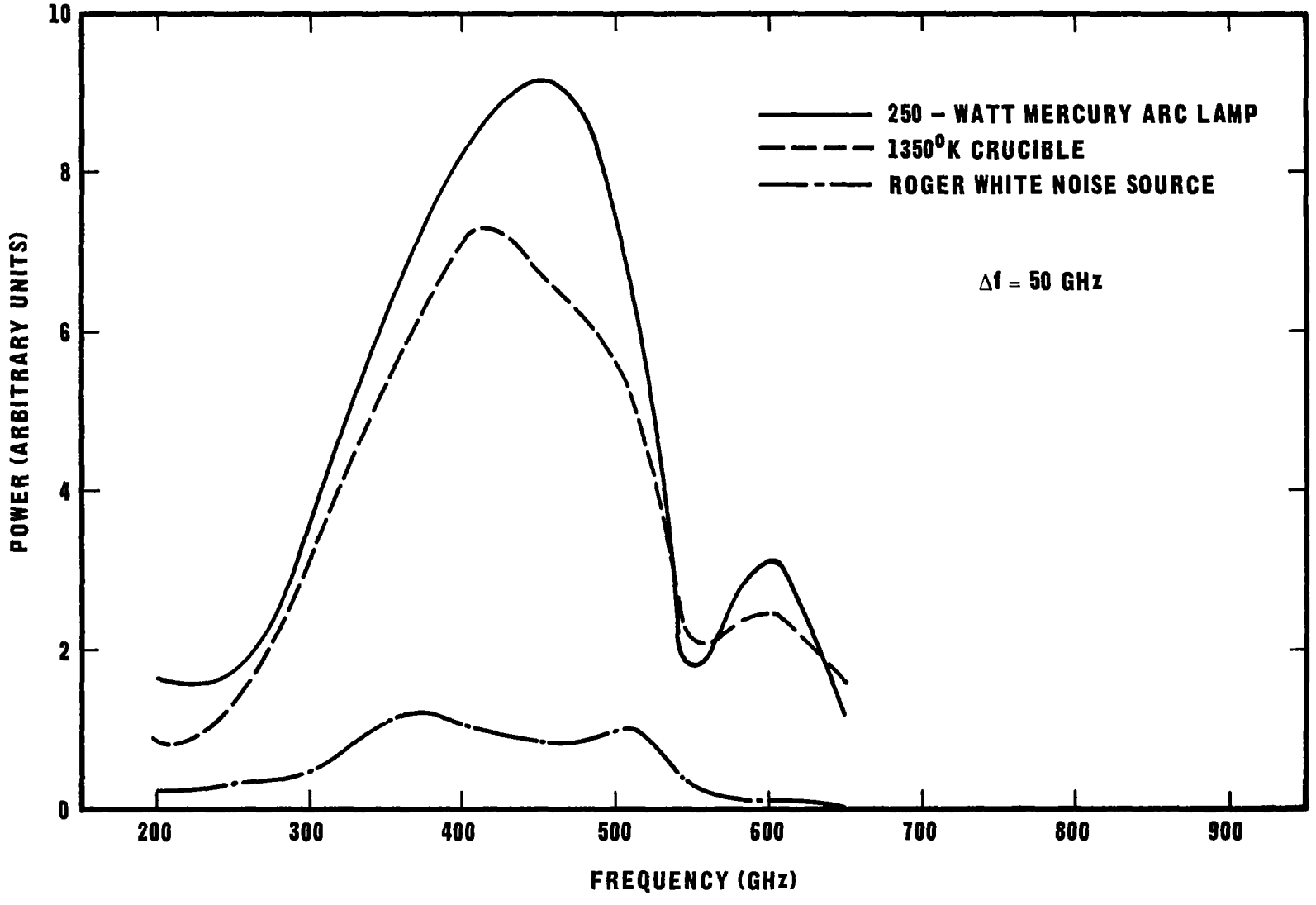

Figure 3. Noise Source Measurements.

The rapid loss in power below 300 GHz is attributed to the following mechanisms: multiple reflections in the 0.0035" thick mica window used on the detector input horn, loss of power carried in high-order modes cut off at low frequencies in the detector waveguide, and reduction in efficiency of the resonant beamsplitter. Loss of power above 500 GHz is due, in addition to significant water vapor absorption near 550 GHz and loss in beamsplitter efficiency, to insertion of a filter consisting of two layers of 0.006" thick black photographic paper.

The effects of black photographic paper* as a filter are seen more clearly in figures 4 and 5. Figure 4 shows spectra calculated in the 450 to 1100 GHz frequency band from data recorded with a mercury arc noise source and a 0.005" thick Mylar beamsplitter. First a reference interferogram was recorded. Then a second interferogram was recorded with a single layer of 0.006" thick black photographic paper placed over the detector horn and a third interferogram was recorded with a second layer of 0.006" thick black photographic paper inserted in the beam at a 45° angle at the input prime focus of the spectrometer optics. Figure 5 shows the transmission/absorption of single sheets of black photographic paper obtained by taking the difference in db of the above two filtered spectra and the reference spectrum.

*The black photographic paper referred to here is the paper used to wrap film by the Kodak Corporation, Rochester, New York.

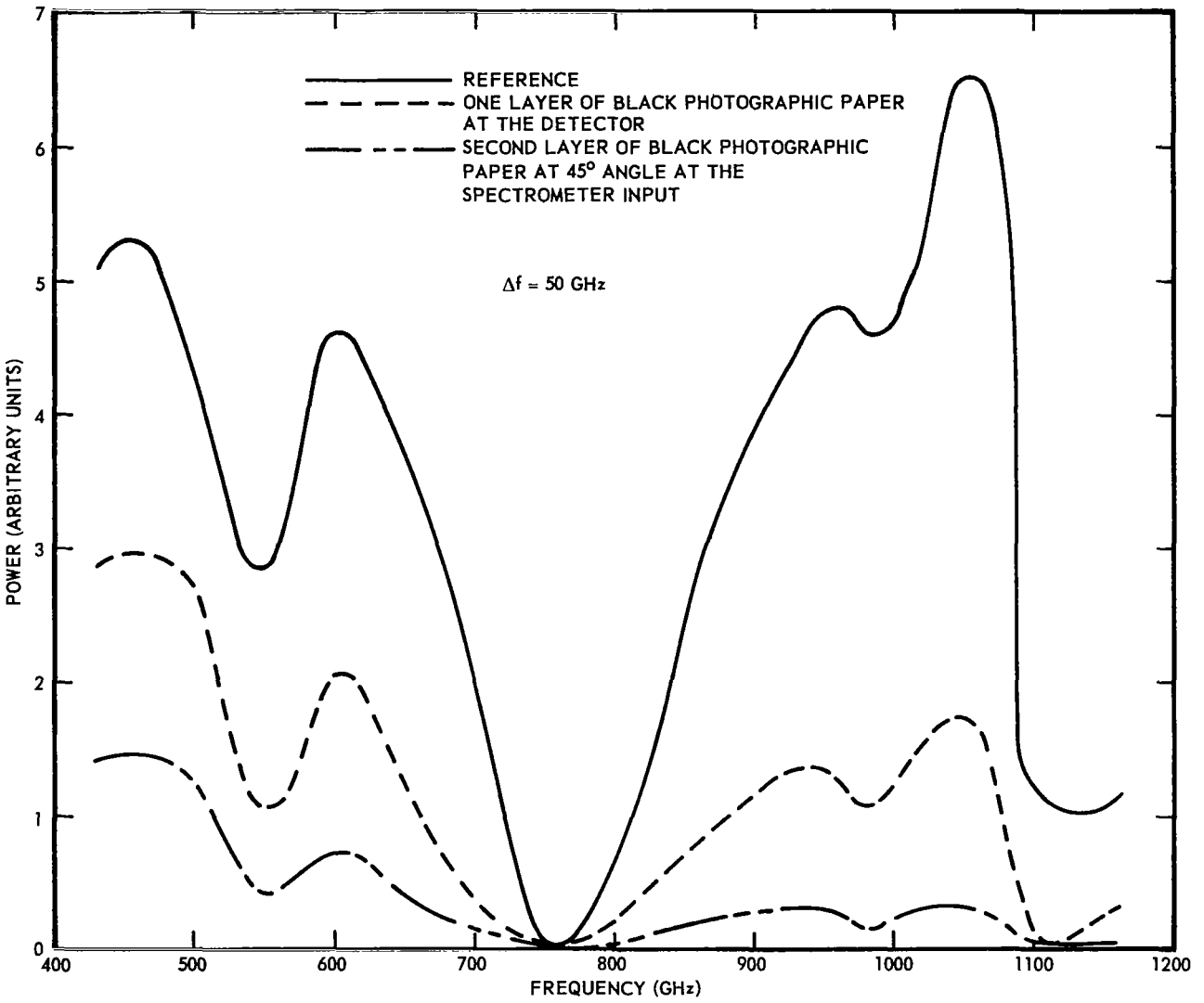

Figure 4. Transmission Spectra for Single Sheets of 0.006" Thick Black Photographic Paper.

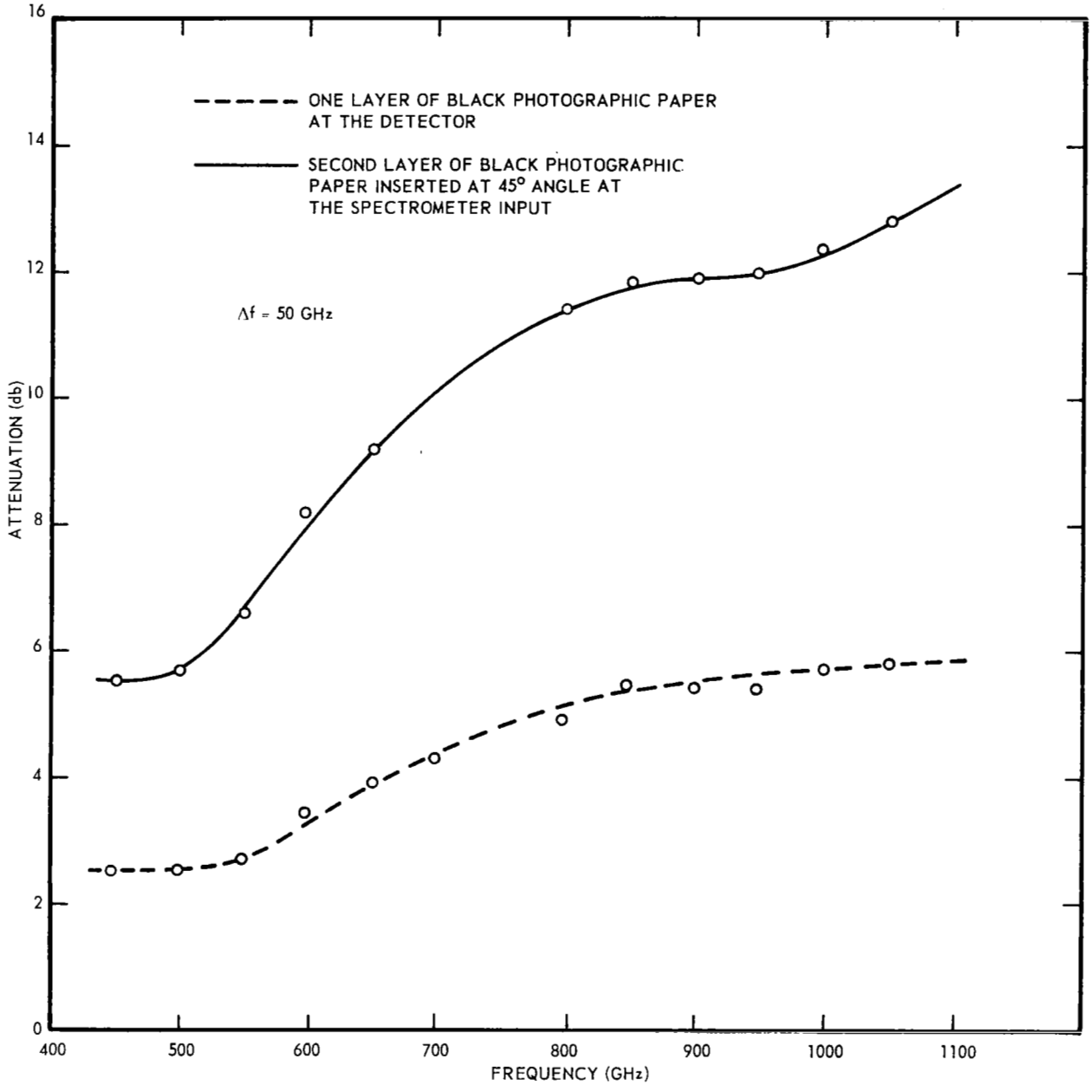

Figure 5. Photographic Paper Absorption Characteristics Calculated from Spectra Shown in Figure 4.

III. GASEOUS ABSORPTION

A number of measurements have been made in the 500 GHz to 1500 GHz frequency band to demonstrate potential use of the spectrometer as a tool for measuring attenuation and bandwidth parameters for gaseous absorption lines. The experiments discussed in this section were chosen for two reasons. One is to show that sufficient resolution is available to measure the characteristic shape of certain water vapor absorption lines. In other examples, it is demonstrated that attenuation measurements can be made by comparing spectra calculated from interferograms recorded through a given sample and in the absence of the sample.

Figure 6 shows a high resolution spectrum which was calculated from an interferogram recorded under normal room atmospheric conditions (50% humidity). The contour of the spectrum indicates that over the effective two-meter path length of the spectrometer water vapor absorption lines can be seen at 915, 970, and 988 GHz. It should be noted that these frequencies are more closely in agreement with calculations given by Yunker and Querfeld [7] than with the calculations by Ghosh and Edwards [8]. The 3.9 GHz resolution used in this spectrum was selected to give an accurate representation of the actual line shape and should not be thought of as maximum resolution for the spectrometer. Resolution, over the normal operating frequency, is limited to about 0.5 GHz by maximum mirror travel and by finite aperture [9].

Spectra calculated from an interferogram recorded with the instrument evacuated to a few torr and a reference interferogram recorded at normal atmospheric conditions are shown in figure 7. An absorption plot calculated by taking the difference in db of the above two spectra is shown in figure 8. The water vapor absorption lines as they occur at normal room temperature, pressure, and humidity with a two-meter effective path length are seen clearly in this figure at 557, 753, 987, 1098-1113, 1161, 1213-27, and 1407 GHz. It also appears that the two lines at 641 GHz, the three lines near 860 GHz and the four lines from 1310-30 GHz are visible. The 1320 GHz cluster are predicted by Ghosh and Edwards [8] to be comparable in magnitude to the 550 GHz line and this is seen to be the case although the line "skirts" are masked by the more intense absorption on either side. Reference 8 predicts eighteen

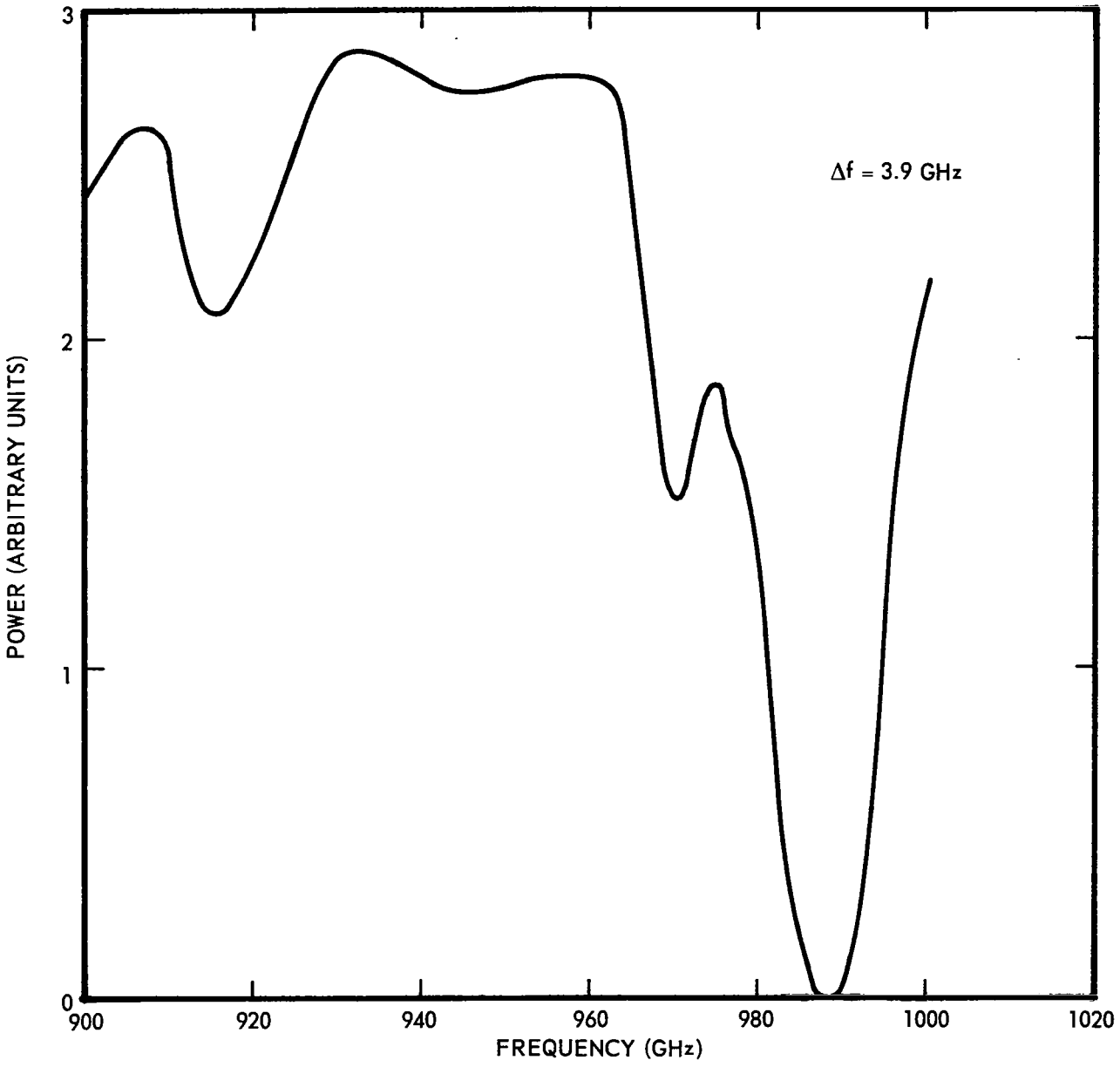

Figure 6. High Resolution Spectrum with 0.005" Thick Beamsplitter and Crucible Source.

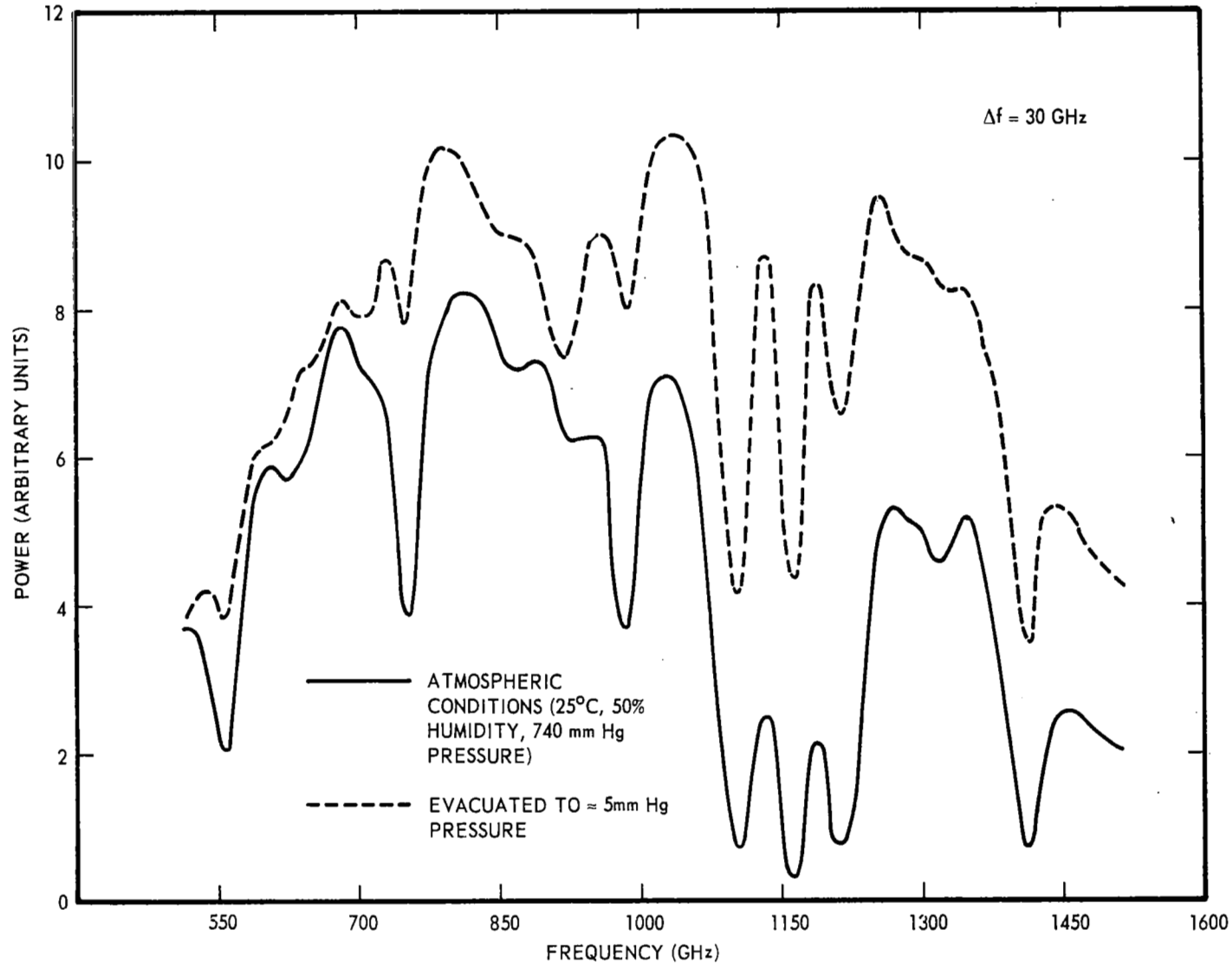

Figure 7. Atmospheric Attenuation Spectra.

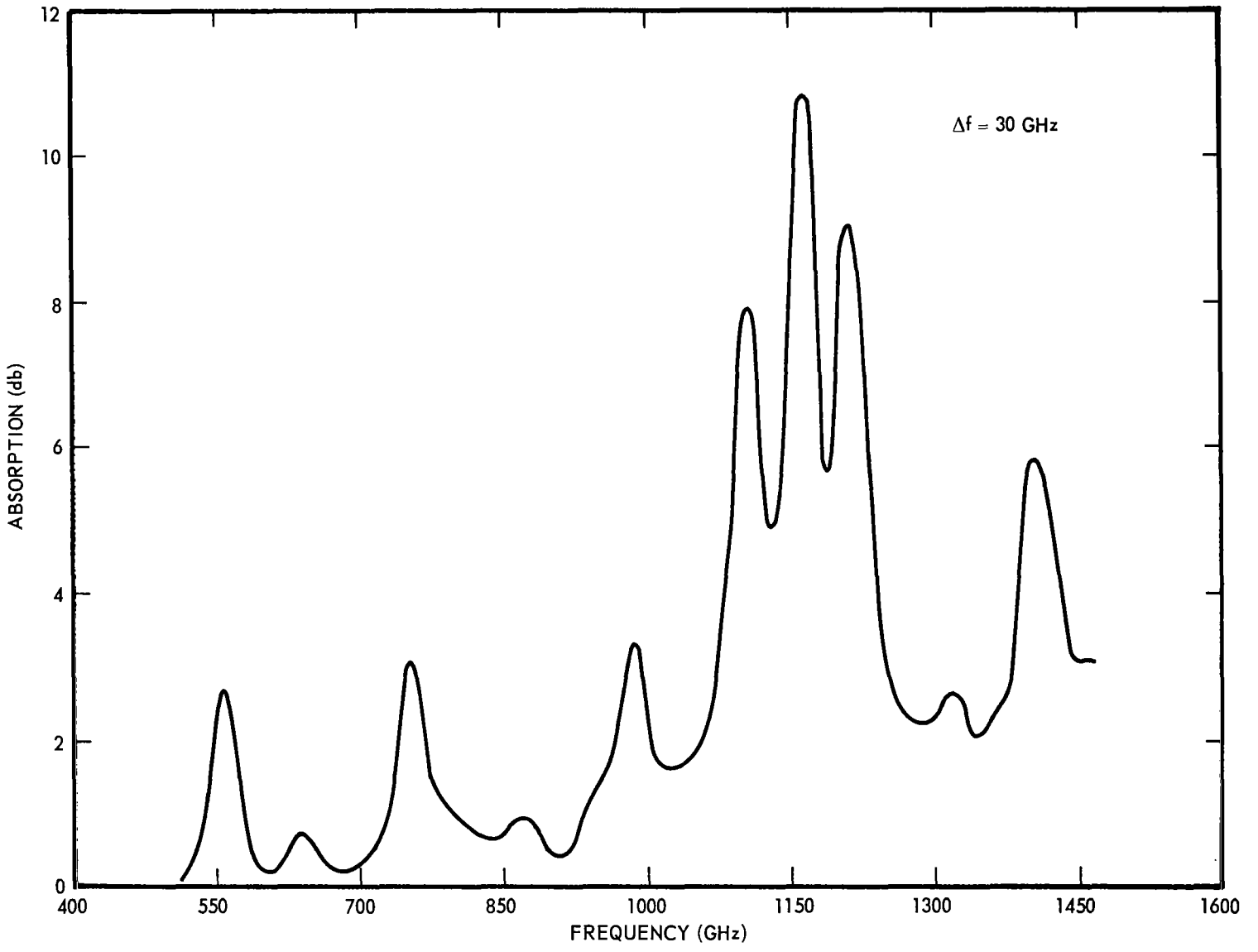

Figure 8. Absorption Spectrum Calculated from Figure 7.

lines from 1000-1250 GHz. These are masked by the very intense lines mentioned above and by the 30 GHz resolution at which this spectrum was taken. With greater resolution the absorption lines would be somewhat greater in magnitude and slightly narrower in bandwidth than shown in figure 8. Sheppard [10] calculated the absorption curve to 1000 GHz on the basis of a 0.2 cm^{-1} shape factor and the Van Vleck-Weisskopf equation. The agreement in the observed values of attenuation in the windows near 600 and 680 GHz is very close to that calculated. Sheppard's curve did not consider values of the lower rotational quantum number $J > 6$, hence the windows observed near 825 and 910 GHz are, as would be expected, greater than calculated. It may be noted that the 753 GHz line is comparable in strength to the 557 GHz line as calculated [8,10] rather than as observed by Iaroslavski and Stanevich [11]. It is not expected that a better vacuum would cause appreciable change in the line skirts or in the weaker lines; however, the peak attenuation of strong lines is probably several decibels greater than shown in figure 8.

IV. THE SPECTROMETER AS AN INSTRUMENT FOR DETERMINING PROPERTIES OF DIELECTRIC SOLIDS

Very little data exist on the relative permittivity or loss tangent of solid dielectric materials above the frequency of 10 GHz. Waveguide and resonant cavities become exceedingly small in the millimeter wavelength region and are not frequently used in the sense of operating in a single dominant mode in the submillimeter wavelength region. Such measurements that are attempted in the millimeter wave region generally utilize the free-space techniques described by Redheffer [12]. The relative dielectric constant is determined by inserting a large area sheet of the unknown material in between a transmitting and receiving horn, one of which can be displaced along a calibrated scale parallel to the principal axis of the horns. For a monochromatic source illuminating a lossless dielectric solid of relative permittivity, ϵ_r, and thickness, d, at normal incidence one may write

$$\epsilon_r = \left(1 + \frac{\delta}{d}\right)^2 , \tag{1}$$

where δ represents the path length difference obtained from the calibrated scale for the air gap with and without sample.

The position of the horns which gives the same effective path length with or without the sample is locatable by a phase comparison of the test transmission path with a reference path in a bridge. This interferometer method can also be implemented in the submillimeter region only in those cases where it is appropriate to use broadband radiation; that is, dispersion of the dielectric samples may reduce the accuracy and usefulness of this method.

Another technique makes use of the resonant properties of a thick dielectric sheet to measure both dielectric constant and loss tangent. It is well known that a material exactly an integral half-wavelength thick, i. e.

$$d = \frac{n\lambda_m}{2} , \tag{2}$$

where λ_m is the wavelength in the material and n is an integer, will transmit

the maximum normal incident energy. For a material with dielectric constant, ϵ_r,

$$\lambda_m = \frac{\lambda_0}{\sqrt{\epsilon_r}} \quad , \tag{3}$$

where λ_0 is the freespace wavelength. Substituting (3) into (2) yields

$$d = \frac{n\lambda_0}{2\sqrt{\epsilon_r}} \tag{4}$$

for the maximum transmission condition.

When this resonance technique is used with the interference spectrometer, there is no difficulty in inserting a sheet of dielectric in the beam, for example, between the source chopper and the succeeding ellipsoidal reflector. An interferogram can be recorded with and without the sample, and two normalized spectra can be obtained. Taking the ratio of these two spectra results in a graph like that shown in figure 9. It may be noted that there are four maximum transmission points on this curve, each corresponding to a particular value of the integer n. The thickness of the sample can be measured rapidly. If one assumes that the material under test has a constant relative permittivity to the nearest tenth over a portion of the frequency range of the spectra, a series of equations like (4) can be written in which ϵ_r is the unknown:

$$\begin{aligned}
\epsilon_r &= \left[\frac{n\,\lambda_{01}}{2d}\right]^2 \\
\epsilon_r &= \left[\frac{(n+1)\,\lambda_{02}}{2d}\right]^2 \\
&\cdots\cdots\cdots \\
\epsilon_r &= \left[\frac{(n+p)\,\lambda_{0p}}{2d}\right]^2 ,
\end{aligned} \tag{5}$$

where $\lambda_{01}, \lambda_{02}, \ldots, \lambda_{0p}$ are the wavelengths corresponding to the maxima

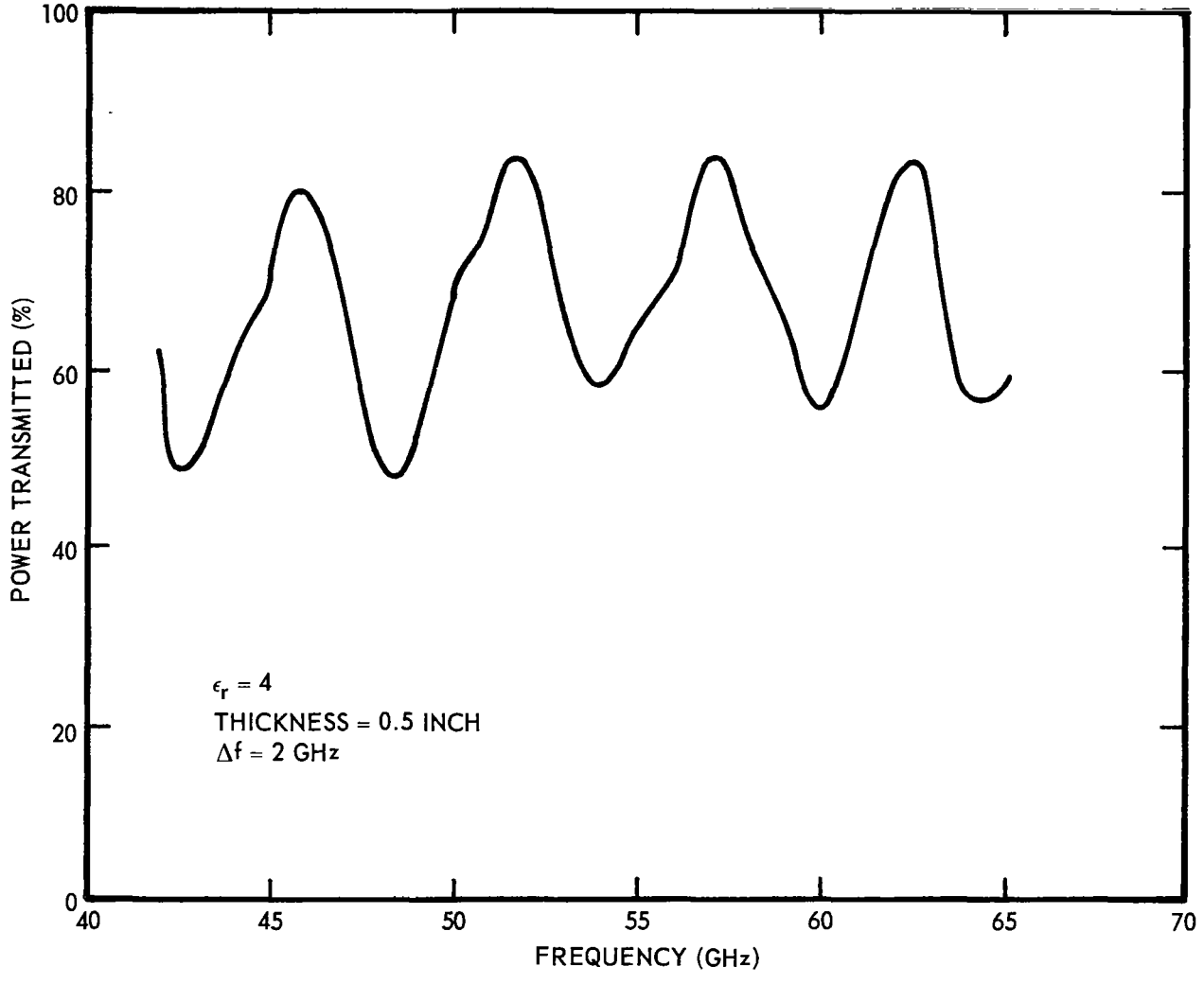

Figure 9. Power Transmission Characteristic of Low-Loss Dielectric Material as a Function of Frequency.

on a graph like figure 9. It is a simple matter to pick the unique value of n that will cause a constant value of ϵ_r to result for the system of equations (5). In executing such a technique, care must be exercised in the total frequency range over which the maxima extend. Very likely, three to five maxima should suffice to give a good picture of the relative dielectric constant of the material in a given frequency region.

Some effort has been spent on relating the free-space relative dielectric constant measurement spectra to determination of sample loss tangent. The spectrum taken with the sample in the path is of lower intensity than the one taken without the sample. Redheffer [12] suggests that the reduction in amplitude of the transmitted wave in the free space technique can be used for loss tangent calculations on certain materials. The equation for this calculation is

$$t = \frac{4\sqrt{\epsilon_r}\ e^{-b}}{(\sqrt{\epsilon_r} + 1)^2 - (\sqrt{\epsilon_r} - 1)^2\ e^{-2b}}\ , \qquad (6)$$

where t is the voltage transmission coefficient (in this case at the spectrum maxima) and $b = 0.5\ \pi n \tan \delta$, where n is an integer as defined in Equation 2 and $\tan \delta$ is the unknown loss tangent. The relative dielectric constant ϵ_r used in Equation 6 is determined first considering the material to be lossless. Iteration is then used to refine the dielectric constant and in turn the loss tangent. For a sample of Stycast* with relative dielectric constant of 3.9 the transmission coefficients changed on each of four maxima so that the loss tangent was observed to center between 0.004 and 0.005 for all the data.

Experimentally, there are definite limitations to the approach. At this reporting, it has not been possible to obtain consistent differences in the spectra with and without the sample when relative permittivity is less than about 3.5. However, the measurements have been confined to sample thickness of one-half inch or less. Redheffer points out difficulties with non-plane wavefronts and diffraction of the sample when using free-space techniques, and these must be either minimized or else taken into account in the measurement procedure.

*Emerson & Cuming, Inc.

V APPENDIX

A. OPERATING INSTRUCTIONS

The purpose of this appendix is to furnish an introduction to the experimental mechanics of Fourier transform spectroscopy. A discussion of rule-of-thumb methods for selecting parameters such as traverse speed, recording time, sampling rate, and time constant is presented along with a discussion on spectrometer alignment and beamsplitter selection. The discussion applies directly to the Michelson interferometer arrangement but can be applied to the wavefront-dividing arrangement of reference 1 by considering that the latter arrangement fully modulates only energy propagated in the lowest order spacial mode and that mirror displacement per differential path length change for the wavefront-dividing arrangement is less than for the Michelson arrangement by a factor of two.

A review of the Fourier transform process similar to the discussion in reference 1, but which considers the apodizing function from a convolution point of view, is included to assist the reader in relating the mathematics of this process to the more common mathematics of basic network theory and to help relate resolution bandwidth to a given apodizing function.

As the driven mirror shown in figure 1 is displaced, the detector response as a function, $V(x)$, of path delay, x, is recorded. This function, which is called the interferogram, is symmetrical in the path delay. The power spectrum, $P(\nu)$, of the radiation detected can be obtained from the interferogram by the Fourier transform,

$$P(\nu) = \int_{-\infty}^{\infty} V(x) \cos\left(\frac{2\pi x \nu}{c}\right) dx = F_{\cos}\{V(x)\}. \tag{1}$$

In practice, $V(x)$ is recorded over a finite differential path length, L, so that the function actually computed is

$$P_1(\nu) = 2\int_{0}^{L} V(x) \cos\left(\frac{2\pi x \nu}{c}\right) dx = \int_{-\infty}^{\infty} a_1(x)\, V(x) \cos\left(\frac{2\pi x \nu}{c}\right) dx$$

$$P_1(\nu) = A_1(\nu) * F_{\cos}\{V(x)\} \tag{2}$$

where the symbol * denotes convolution, and $A_1(\nu)$ is given by

$$A_1(\nu) = 2L \left[\frac{\sin (2\pi\nu L/c)}{2\pi\nu L/c}\right] \quad . \tag{3}$$

This function, $A_1(\nu)$, has bandwidth of only $\Delta_1 = 0.6\ c/L$, but has undesirable sidelobes which are on the order of 25 per cent of the main peak. In order to reduce these sidelobes, the function $a_1(x)$ can be replaced by the function

$$a_2(x) = \begin{cases} 1 - |x|/L\ , & (-L \leq x \leq L) \\ 0\ , & (x < -L,\ x > L) \end{cases} \tag{4}$$

so that

$$A_2(\nu) = F_{\cos}\{a_2(x)\} = L \left[\frac{\sin^2 (\pi\nu L/c)}{(\pi\nu L/c)^2}\right] \tag{5}$$

has increased bandwidth, $\Delta \approx c/L$, but sidelobes are reduced to about 6 per cent of the peak.

In all of the examples presented in this report, the apodizing function given by Equation (4) was used, and the numerical integration performed by the computer was

$$P(\nu) = \tfrac{1}{2}V_m + \sum_{k=1}^{N} V_{m+k}\ a_2(x_k) \cos (k2\pi\delta\nu/c) \tag{6}$$

resulting in a resolution bandwidth of $\Delta \approx c/L$. In Equation (6), the index m denotes the data point which occurs at the zero point of the interferogram, and δ is the increment in x.

In establishing the parameters for a particular interferogram, resolution bandwidth must be considered first. The degree of detail in a power spectrum is limited by resolution bandwidth in a manner analogous to the rise-time limitations of a low pass filter. After the necessary resolution bandwidth has been established, the corresponding mirror displacement, D, can be calculated from $\Delta = c/L$ and $L = 2D$.

The minimum total recording time, T, for obtaining data for a power spectrum with a given resolution and known maximum frequency is limited by the maximum recording speed of the tape punch which is presently about one sample per second, and the maximum total recording time is limited by the six-hour hold time of the cryogenic detector. Another factor to be considered in selecting total recording time for an interferogram is that signal-to-noise ratio is directly proportional to the square root of this parameter for a spectrum of given resolution. It is, therefore, advisable to make total recording time as long as possible within acceptable limits whenever signal-to-noise ratio is to be marginal for an experiment.

After establishing values for T and D, velocity of mirror displacement is found from $S = D/T$, and the proper gear ratio and motor speed can be selected.

Sampling theory dictates that the maximum sampling interval, t_s, must be no greater than $\frac{1}{2}(\lambda_m/S)$, where λ_m is the wavelength corresponding to the highest frequency of interest in the power spectrum to be calculated. In the past, the sampling interval for a given interferogram has been selected by simply driving the instrument through the first few cyclic variations at the desired mirror displacement velocity and picking a sampling frequency which would give about ten data points per cycle; that is, $t_s = 0.1\ \lambda_m/S$. This method gives a sampling frequency which adequately describes the information and, at the same time, provides a margin of safety of about a factor of five over the calculated minimum sampling frequency to prevent image frequency overlap.

Two additional considerations in selecting an optimum sampling frequency follow: 1) With the present computer program, it is necessary to select a data point as the zero phase difference point of the interferogram rather than interpolate between points, thus one's ability to accurately select the zero point and to avoid an undesirable baseline shift as discussed in reference 13 is limited by the density of available data points. 2) Computer time and, hence, cost required to calculate a given number of spectral points is roughly proportional to the number of data points in the interferogram.

Detection integrating time constant, τ, must be selected so that no appreciable attenuation is seen at the frequencies of interest, while higher

order frequencies are adequately suppressed to avoid image frequency distortion. It can be shown [13] that the above requirements are usually satisfied if one selects $\tau \approx t_s$. This rule-of-thumb selection has been used in virtually all of the experiments in this report.

EXAMPLE:

For the interferogram shown in figure 10, the following parameters were selected: D = 3.86 cm, T = 5830 seconds, t_s = 2.4 seconds, τ = 1 second, $\Delta\nu \approx 4$ GHz. Note the slight asymmetry of the data points about the central maximum in the interferogram in figure 10. This asymmetry indicates an error in selection of the zero phase difference point, and a corresponding base line shift is evidenced by the negative power level at higher frequencies in the calculated power spectrum shown in figure 11. The appreciable loss in power between 600 and 900 GHz is due to a beamsplitter null as discussed below.

Before the spectrometer can be aligned, an adequate noise source and detector and a beamsplitter must be selected. A 4 to 5 db transmission loss will be experienced when the instrument is properly aligned, so a source and detector which will give a minimum signal-to-noise ratio of 15 db or more should be selected. In the past, the Roger White neon source and evacuated barretter discussed on page 3 have been used for preliminary alignment in order to avoid unnecessary use of liquid helium. It has also been found to be somewhat easier to align the instrument first at the longer wavelengths rather than at the submillimeter wavelengths at which the liquid helium cooled bolometer is most sensitive.

The Michelson arrangement discussed in this appendix uses a Mylar beamsplitter similar to the one described by Richards [9]. Curves shown in figure 12 can be used as a guide in selecting the beamsplitter thickness for a given frequency band. Plot (a) shows the beamsplitter efficiency for a Mylar sheet of arbitrary thickness and plot (b) shows the 3 db and first null frequencies as a function of beamsplitter thickness.

EXAMPLE:

For a 0.005" thick beamsplitter, the pass band is from 130 to 620 GHz and the first null is at 750 GHz. Figure 11 illustrates

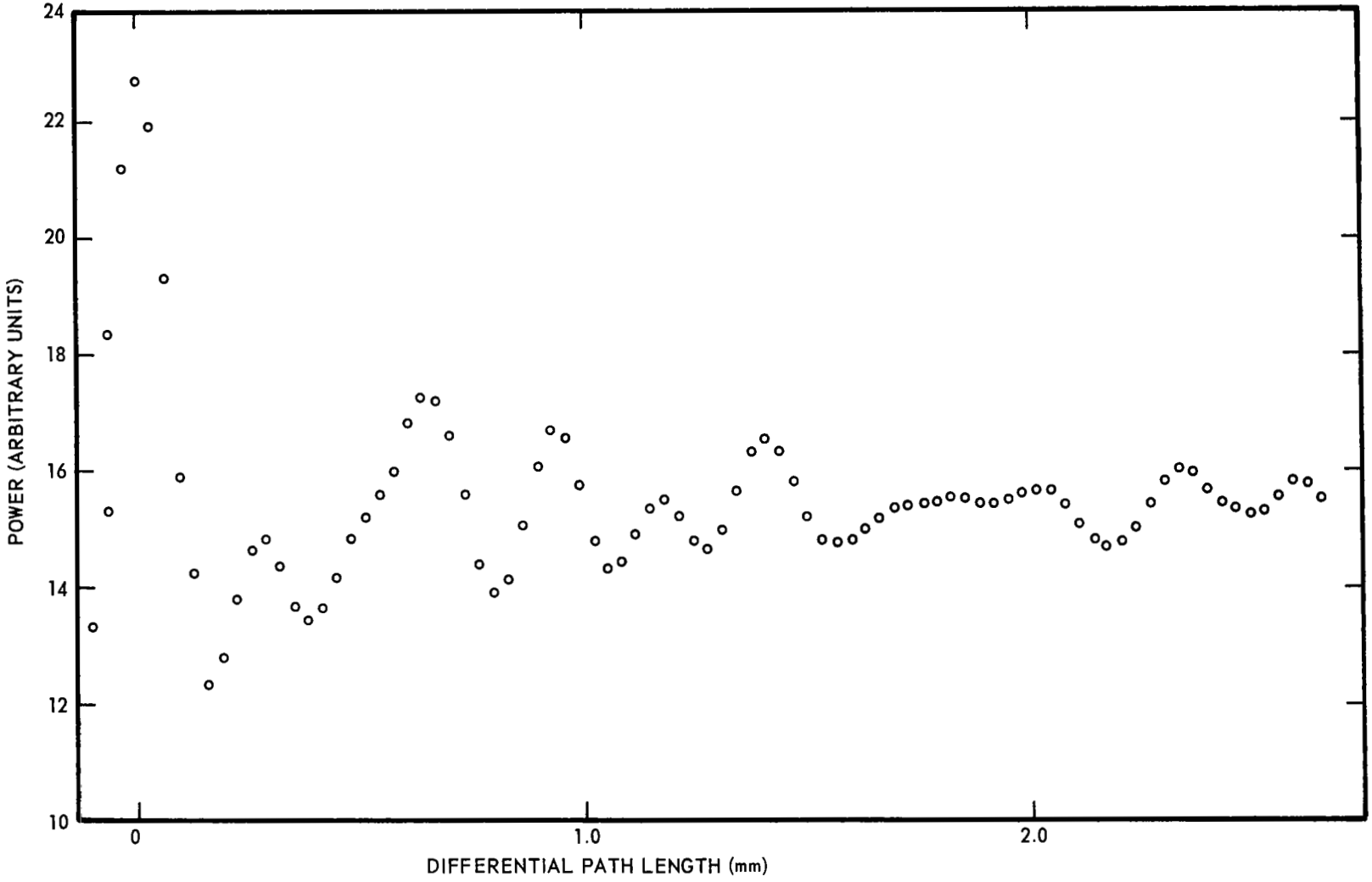

Figure 10. Portion of Interferogram.

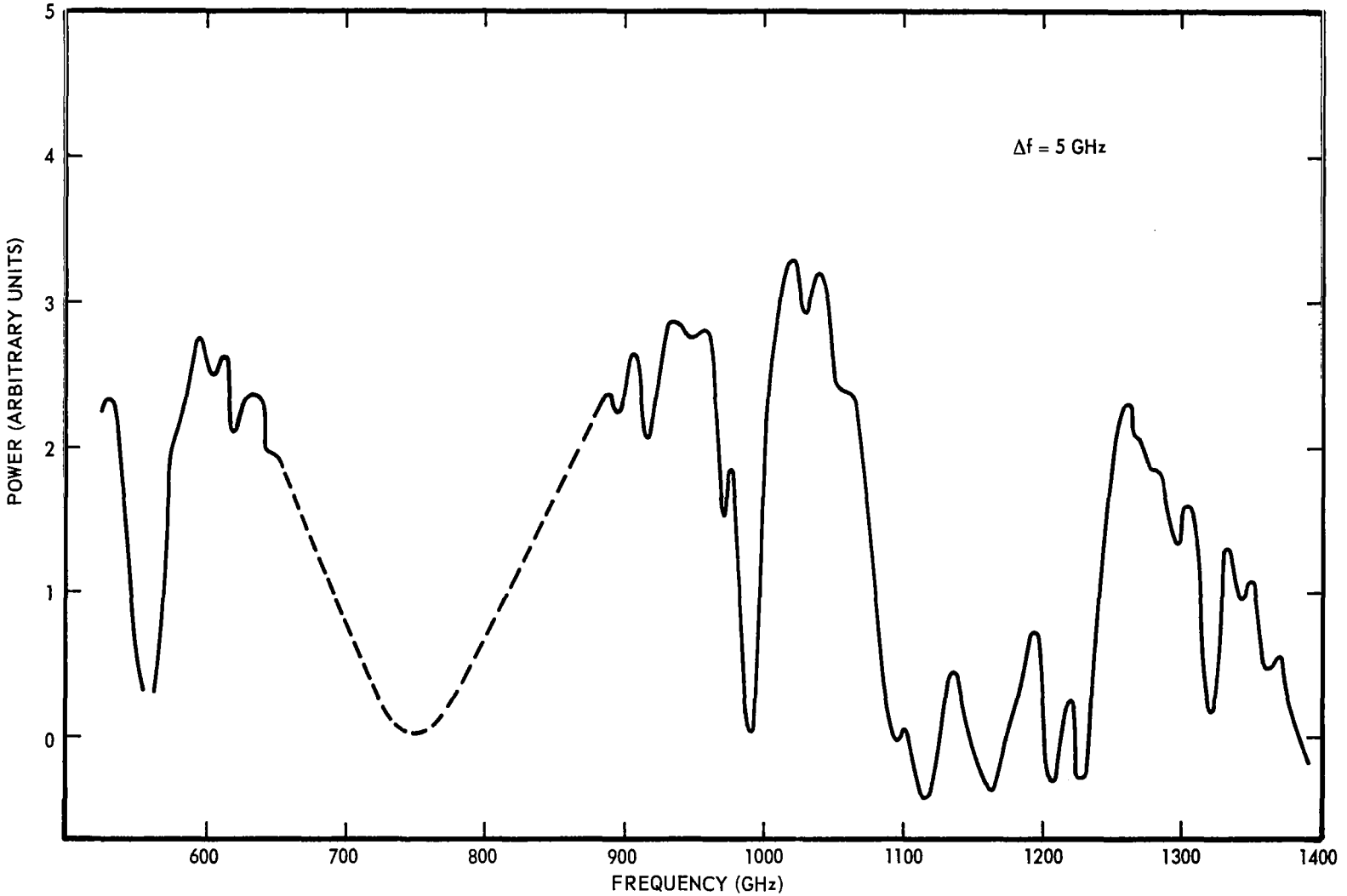

Figure 11. Spectrum Using Crucible Source With 0.005" Thick Beamsplitter (Envelope of Beamsplitter Null Region is Shown Dotted).

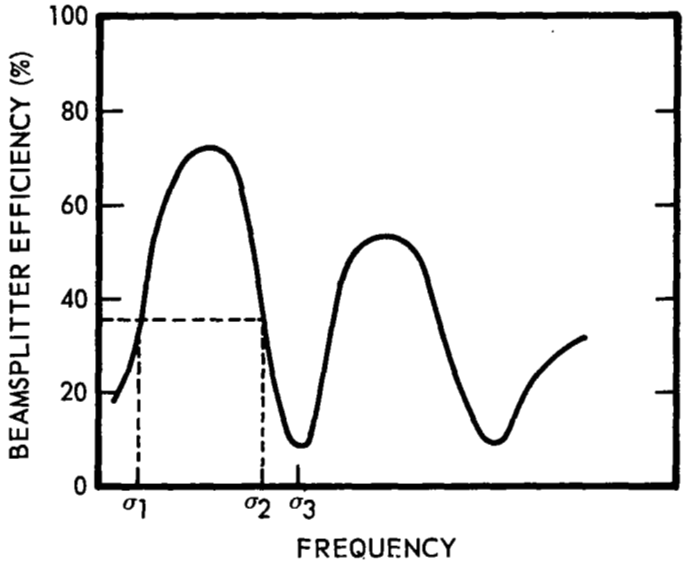

(a)

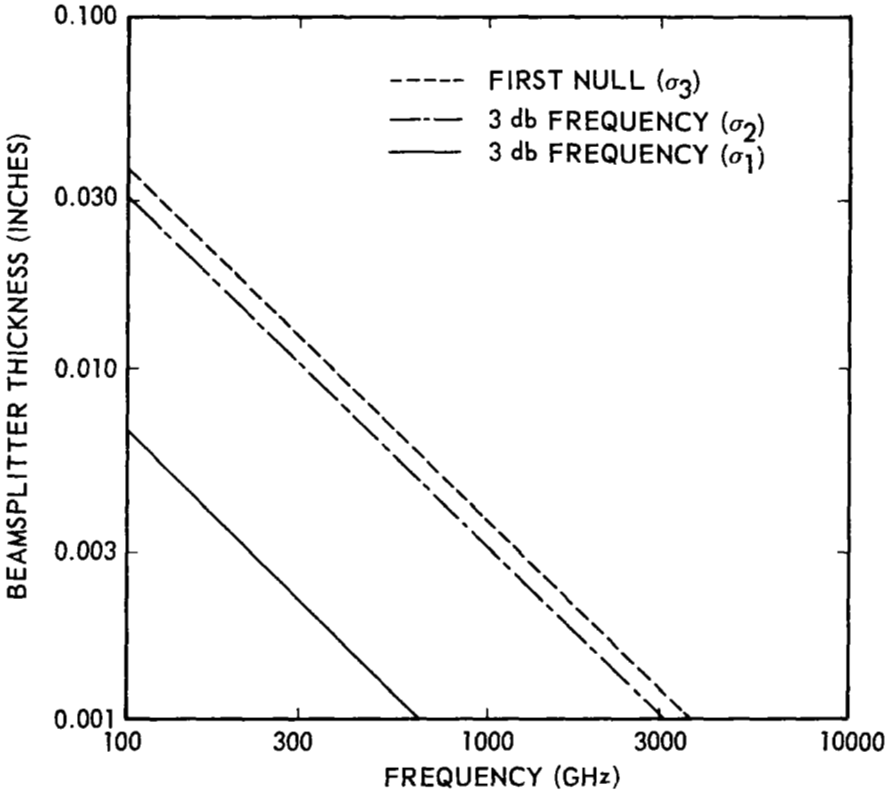

(b)

Figure 12. Beamsplitter Efficiency as a Function of Thickness and Frequency.

a power spectrum recorded with a 0.005" thick beamsplitter. The dotted portion of this plot shows the envelope of the spectrum in the 650 to 875 GHz frequency band which is appreciably attenuated by the predicted beamsplitter null at 750 GHz.

After a source and detector and a beamsplitter have been selected, the instrument can be aligned. One should first lay out the instrument (omitting the source optics) by measuring the distance between mirrors and the desired 45° angles. It is then possible to make use of the known focal characteristics of the twelve inch f:1 system to align the instrument optically with a visible light source. After the system is optically aligned, a noise source can be placed behind a 30 cps chopper at the input slit and the detected signal can be peaked up by making fine adjustments in all mirrors. The beamsplitter is aligned by alternately adjusting the mirror traverse to locate the central maximum and adjusting the beamsplitter angles until a maximum of detector output is reached. The source optics can then be added, and adjusted.

B. LOW TEMPERATURE DETECTOR

In order to extend the operating frequency of the spectrometer to submillimeter wavelengths, a Texas Instruments liquid helium cooled germanium bolometer was obtained. Useful experience has been gained in the process of modifying this cryogenic detector for submillimeter operation and designing and installing necessary bias circuitry to couple the germanium bolometer to a parametric amplifier. The object of this appendix will be to briefly discuss some of the problems encountered in the use of this cryogenic detector with the hope that others may profit from this record of experience.

To establish correct parameters (see table I) for the detector bias circuit, the dc measurements shown in figure 13 were made at 4.2° K. The corresponding calculations shown in table II show that the selected load line gives responsivity of 2.2×10^{5} volts/watt and static resistance of 575 K at the operating point. The selected Texas Instruments model RA-3A parametric amplifier provides a nominal gain of 2500, 3 db bandwidth 0.01 to 500 Hz, and equivalent input noise less than 0.05 microvolts rms (0.8 to 10 Hz) according to the manufacturer. It was found necessary to mount this amplifier and the associated circuitry shown in figure 14 inside a Minibox which was then bolted to the side of the cryoflask in order to avoid excessive pick-up and microphonic noise.

A cross section of the low temperature detector in its original form is shown in figure 15. The 1.5 mm x 1.5 mm x 0.002 mm gallium-doped germanium flake is mounted by small wires to a substrate which is thermally connected to the liquid helium container. The irtran window shown in this figure has been replaced by an appropriate waveguide connection. The two methods considered for making this waveguide connection to the germanium element without introducing an excessive heat leak were to use a continuous-thin-walled stainless steel waveguide or to use electroplated tapers which could be mounted with a gap between the inner and outer tapers as shown in figure 16. The latter method was selected as that offering the lowest transmission loss and the easiest fabrication. It was thought that the tapers could be mounted adjacent at room temperature and pressure and that thermal contraction of the helium flask would give a sufficient gap when the inner taper was cooled to

TABLE I

DC PARAMETERS OF CRYOGENIC BOLOMETER

Quantity	Definition	Units
E	Voltage across the bolometer element	Volts
I	Current through the bolometer element	Microamps
$Z = \frac{\Delta E}{\Delta I}$	Dynamic resistance	Megohms
$R = E/I$	Static resistance	Megohms
$S = dE/dQ$*	Responsivity	Megavolts/ watt

* $S = dE/dQ = \frac{Z-R}{2E}$

TABLE II

WORK SHEET FOR DC BOLOMETER MEASUREMENTS*

I	1.0	1.1	1.2	1.3	1.4	1.5	1.6
E	0.660	0.698	0.730	0.758	0.780	0.801	0.820
ΔE		0.070	0.060	0.050	0.043	0.040	
ΔI		0.2	0.2	0.2	0.2	0.2	
R		0.635	0.609	0.583	0.557	0.535	
Z		0.350	0.300	0.250	0.215	0.200	
S		0.204	0.206	0.220	0.219	0.209	

* Temperature = 4.2° K

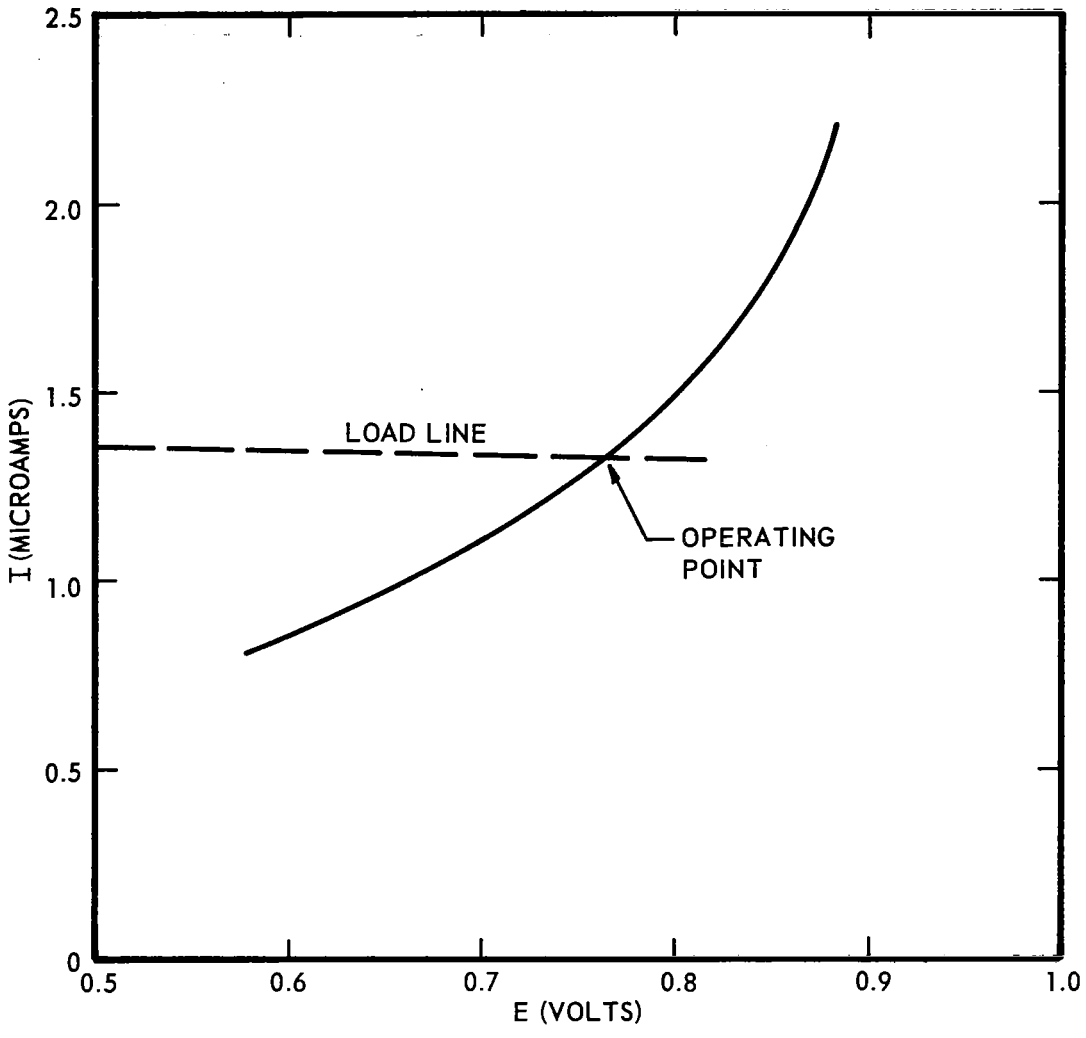

Figure 13. Load Line and dc Characteristics for Germanium Bolometer.

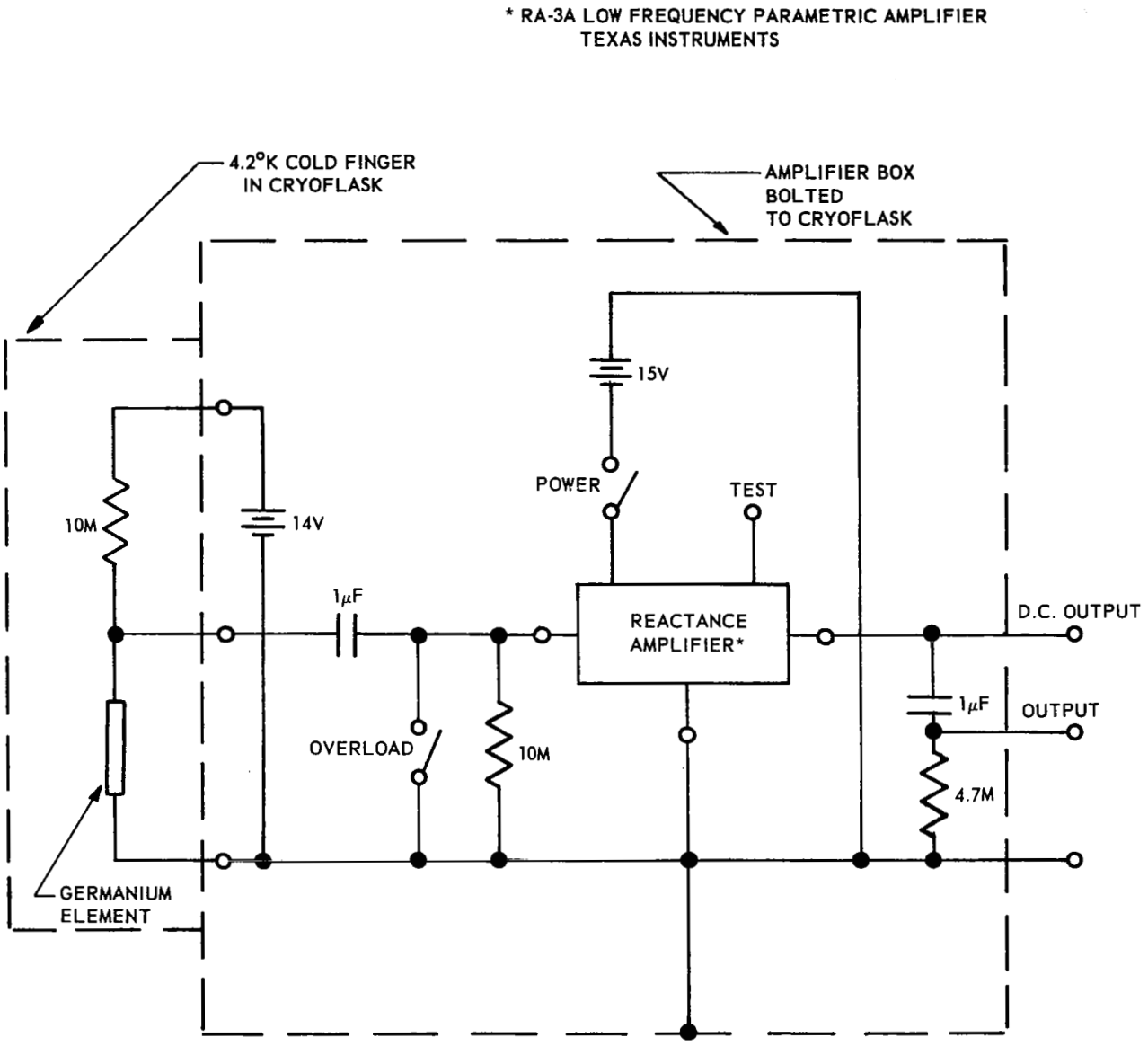

Figure 14. Bolometer Bias and Parametric Amplifier Circuit.

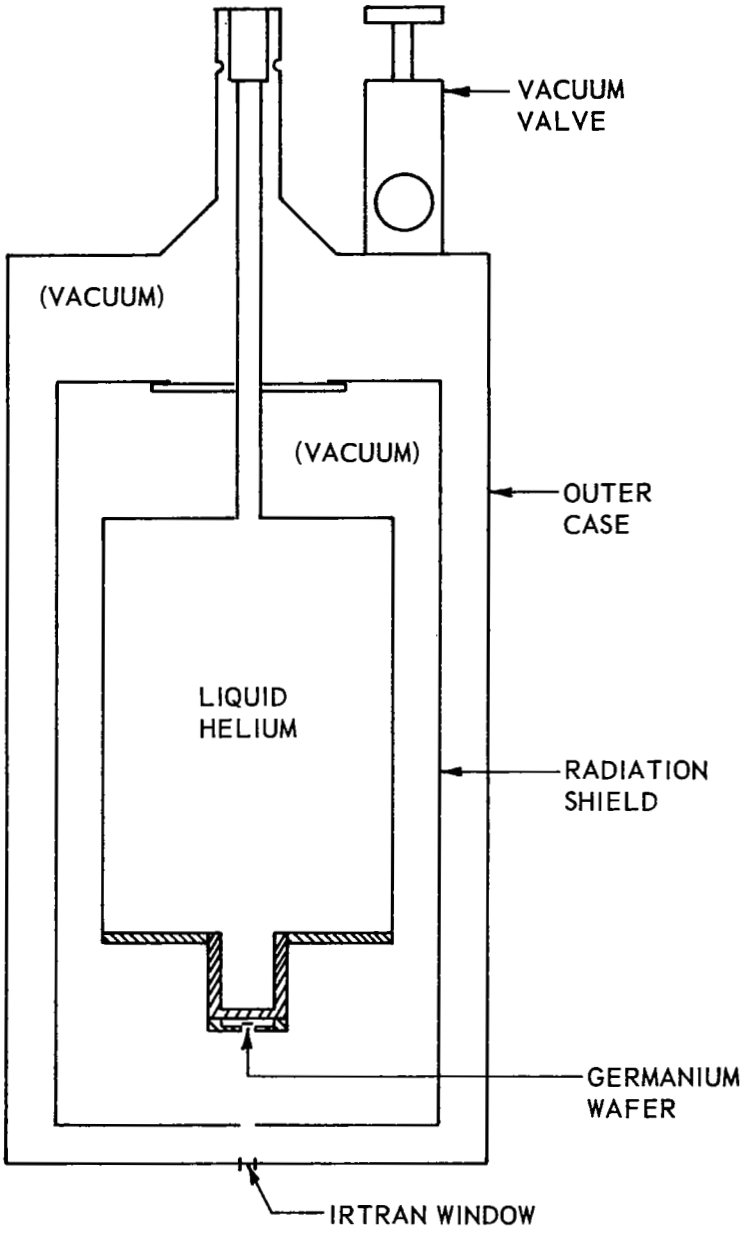

Figure 15. Cross Section of Cryogenic Detector Before Modifications.

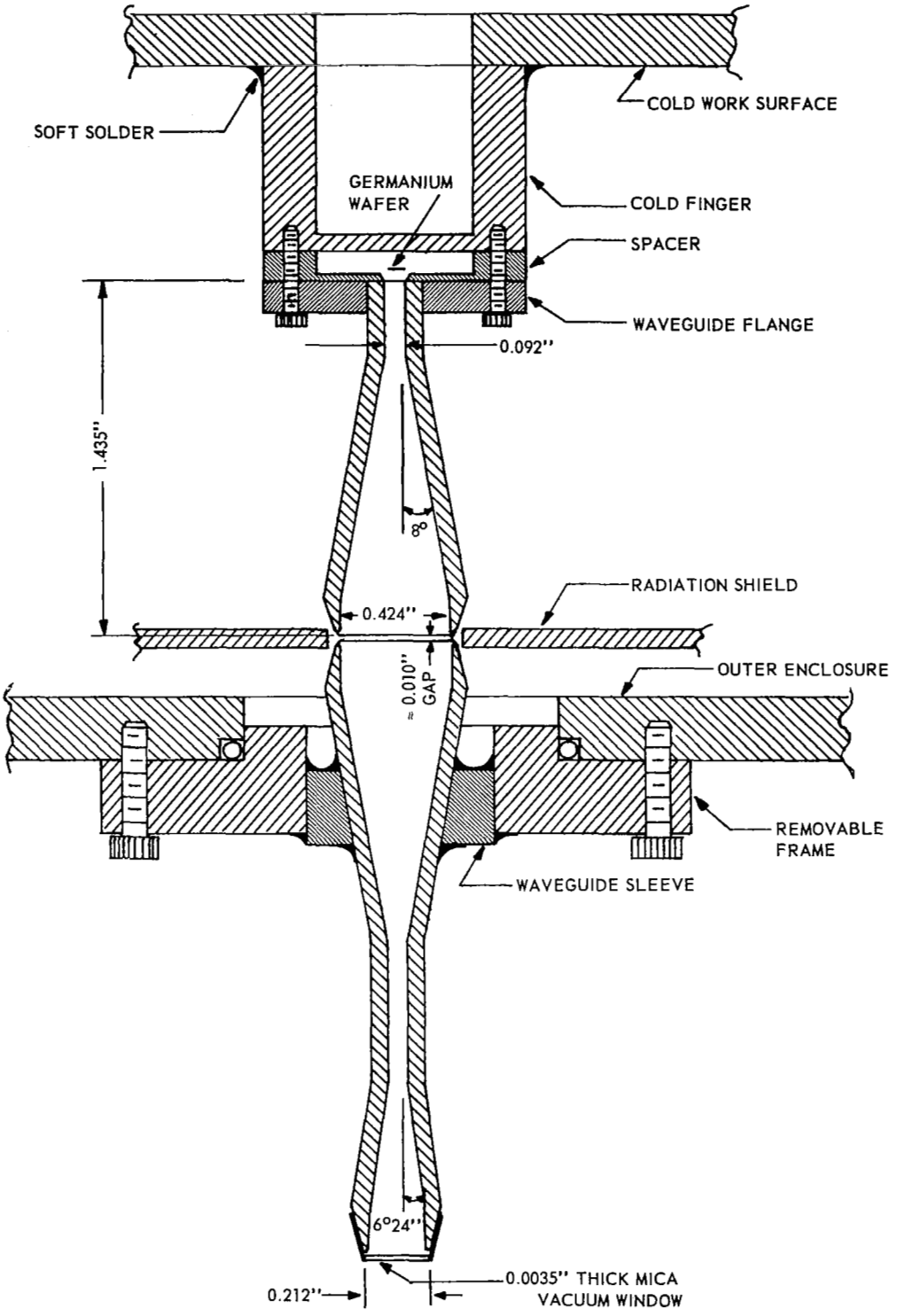

Figure 16. Waveguide Coupling in Cryogenic Detector.

4.2° K. It was found, however, that the problem of selecting a correct gap distance was complicated by mechanical distortion of the container caused by evacuating the outer jacket. The gap distance was eventually set at approximately 0.010 inches, at room temperature and pressure, by trial-and-error methods.

The installation of waveguide tapers for radiation coupling introduced a problem of selecting a vacuum window for the outer taper and introduced an additional heat leak problem. A drop of epoxy was initially used in the throat of the outer horn for a vacuum seal; the epoxy, however, was found to give prohibitively high losses so it was replaced by a 0.0035" thick sheet of mica which was bonded to the outer edge of the horn. In spite of precautions against thermal conduction, maximum hold time was found to be reduced by about a factor of two below advertised hold time of 14 hours after the copper tapers were installed. Approximate calculations, made by considering surface emissivity of the tapers to be 0.5, indicate that radiative heat transfer between the tapers is about the same (27 mw) as the summation of all other significant contributions to heat transfer. Loss in maximum hold time might therefore be attributed to addition of the necessary 0.5 inch diameter hole in the heat shield required by the waveguide tapers.

An additional vacuum problem was encountered when attempts were made to evacuate the atmosphere surrounding the detector and spectrometer so that comparative water vapor absorption measurements could be made. It was found that evacuating the surrounding atmosphere to a few torr relieves pressure which is necessary to form a seal at the vacuum valve, thus allowing the cryogenic vacuum chamber to neutralize with the surrounding pressure. This problem was temporarily circumvented by venting the vacuum valve to atmospheric pressure.

VI BIBLIOGRAPHY

1. Rivers, Wayne K., Jr., A Submillimeter Interference Spectrometer, Final Technical Report, National Aeronautics and Space Administration Research Grant NsG-258-62, Georgia Institute of Technology, 8 May 1964

2. Michelson, A. A., "On the Application of Interference Methods to Spectroscopic Measurements," Phil. Mag. 31, 338 (1891)

3. Fellgett, P., Thesis, Cambridge University (1951)

4. Strong, J., "Interferometry for the Far Infrared," J. O. S. A. 47, 354, (1957)

5. Strong, J., and Vanasse, G., "Interferometric Spectroscopy in the Far Infrared," J. O. S. A. 49, 844 (1959)

6. Strong, J., Concepts of Classical Optics, W. H. Freeman and Company, San Francisco (1958)

7. Yunker, W. and Querfeld, C., Pure Rotational Spectrum of Water Vapor I. Table of Line Parameters, White Sands Missile Range, New Mexico, February 1963

8. Ghosh, S. N. and Edwards, H. D., Rotational Frequencies and Absorption Coefficients of Atmospheric Gases, Air Force Cambridge Research Center, Bedford, Massachusetts, March 1956

9. Richards, P. L., "High-Resolution Fourier Transform Spectroscopy in the Far-Infrared," J. Opt. Soc. Am. 54, 1474, December 1964

10. Sheppard, A. P., Atmospheric Attenuation in the Millimeter and Submillimeter Wavelength Region, Proc. Ninth Annual East Coast Conference on Aerospace and Navigational Electronics, October 1962, p. 6.2.2-1

11. Iaroslavski, N. G., and Stanevich, A. E., "Rotational Spectrum of Water Vapor and Absorption of Humid Air in the 40-2500 micron Wavelength Region," Optics and Spectroscopy 6, 521, June 1959

12. Redheffer, R. M., "The Measurement of Dielectric Constants," Technique of Microwave Measurements, ed. by Carol G. Montgomery, New York: McGraw-Hill Book Company, 1947, 561-676

13. Connes, J., "Spectroscopic Studies Using Fourier Transformations," Revue d'Optique, vol. 40, 1961, 45, 116, 171, 231. (Translated as NAVWEPS Report 8099, Naval Ordnance Test Station, China Lake, California. DDC AD 409 869).